1999

Importance of Convection and Damping on Rates of Convergence for the Lax-Wendroff Method

Joseph Kolibal
University of Southern Mississippi, kolibal@eos.usm.edu

SIAM J. SCI. COMPUT.
Vol. 20, No. 4, pp. 1513–1529

IMPORTANCE OF CONVECTION AND DAMPING ON RATES OF CONVERGENCE FOR THE LAX–WENDROFF METHOD*

JOSEPH KOLIBAL†

Abstract. It is well known that in solving steady state problems using hyperbolic time-stepping methods the intent is to drive the transients to zero as quickly as possible. In this paper the convergence to steady state of the Lax–Wendroff method applied to solving the equations of gas dynamics is analyzed for the Laval nozzle problem by comparing the relative rates of damping and convection using a linearized eigenmode analysis. This analysis is developed for the simpler isenthalpic system and then extended to the full Euler equations. Finally, this allows a comparison between these systems. For both models, useful analytical information can be gleaned about the transient behavior of these systems, especially in regard to quantifying the competitive factors affecting the removal of unsteady waves.

Key words. compressible fluids, algorithm analysis, convergence rates

AMS subject classifications. 76N10, 68Q25

PII. S1064827597308269

1. Background.

Explicit, iterative finite volume methods of the type developed by Ni [16] and Jameson [8] have been examined extensively [5, 9, 11, 10, 13, 15, 19, 21]. The success of these methods in computing steady state solutions to inviscid, compressible flow problems is partly attributable to their algorithmic simplicity, making minimal demands on computer memory, and making efficient use of current architectures. Furthermore by time stepping, the evolutionary behavior of the system is advantageously utilized to obtain weak solutions to problems in transonic flows. Unfortunately, the convergence to steady state of explicit methods can be slow, necessitating the development of numerical techniques [7, 12] to enhance the rate of convergence. The performance enhancements made to Euler solvers have sought through various methods such as multigrid [1] both to improve the damping and convection rates of the numerical scheme and as in the case of nonreflective boundary conditions, to improve the convection of waves by mitigating the reflection of unsteady waves back into the computational domain [2, 6, 20].

A very different method for improving convergence rates to steady state was introduced by Veuillot and Viviand [24, 25, 28]. In this approach, consideration was given to modifying the transient system of equations describing the conservation of mass, momentum, and energy: Assuming that the total enthalpy H is constant along streamlines, the energy equation can be eliminated from the full system of equations. Since this assumption is valid at steady state, both systems describe the same steady state solution. This modification of the transient computation to accelerate convergence is similar to other techniques, for example, the use of local time stepping in which the solution is advanced based on the maximum local CFL number; however, the model equations themselves are modified, not just the numerical scheme.

*Received by the editors April 21, 1997; accepted for publication (in revised form) September 19, 1997; published electronically April 14, 1999.
http://www.siam.org/journals/sisc/20-4/30826.html
†Department of Mathematics, University of Southern Mississippi, Hattiesburg, MS 39406 (kolibal@eos.st.usm.edu).

Using the isenthalpic system, or H-system, produces some gain in efficiency over the full system of equations by having one less equation to carry along computationally. In practice this savings amounts at best to only a slight gain in efficiency in contrast to results which showed that the isenthalpic system indeed does converge in fewer iterations to steady state than the full system using local time stepping. This improvement was often explained by noting that the H-system, lacking an energy equation, is in some sense constrained by having one less degree of freedom. Although intuitively appealing, there is no compelling argument why a constrained system should converge any faster than one which is not constrained. The appealing aspect of the isenthalpic system from the viewpoint of convergence analysis is that it introduces a simpler, alternative transient model which can be used to study convergence to steady state.

In this study, the intent is to use the isenthalpic system to study the comparative effects of damping and convection on the convergence of the Lax–Wendroff scheme. Having only two eigenvalues, the isenthalpic model is comparatively easy to work with, in contrast to the full Euler system which has three eigenvalues in one dimension. Working with both models leads to a better understanding of why using the isenthalpic system to solve pseudotransient problems, i.e., those involving local time stepping, showed initial promise for accelerating the convergence to steady state. Although alternative models are no longer being actively investigated for improving the convergence of explicit methods for solving the Euler equations, the use of comparative pseudotransient systems to study the mechanisms for quenching transient waves is still important and can provide a useful tool for studying convergence properties of numerical schemes, at least where it is possible to accomplish a useful linearization.

The basis for this analysis rests on an application of a linearized wave model to study the convergence rates to steady state of the Lax–Wendroff method (LW). By comparing two pseudotransient models, the competitive role that the eigenvalues take in determining the effectiveness of the numerical update in damping unsteady waves, relative to their convection from the domain, leads to analytical predictions of the relative convergence rates. These analytical predictions can be tested against numerical studies. This analysis shows that the convergence of the H-system can be understood in part through its impact on shifting the eigenvalues of the system during the transient so as to produce greatly improved convergence at Mach numbers much less than 1/2. For low-Mach-number transonic problems, typical of many of those examined in the early 1980s, this analysis shows that using the isenthalpic model would yield improvements in convergence; on moving to higher Mach numbers, this benefit is not as easily sustained. Furthermore, if the H-system is constrained in any sense relative to the full system containing an energy equation, it is precisely because the eigenvalues of the H-system are constrained to values which improve the convergence properties of the numerical update.

This work is motivated by the wavelike properties of the transient solution exhibited during the transition to steady state which has been studied extensively by several researchers [22, 26, 27]. While eigenmode analysis has been used extensively to assess the accuracy and stability of LW using finite volume schemes [3, 4], comparatively little work has been done on convergence [18] and a complete assessment of the convergence rates of explicit iterative algorithms is far from complete.

2. A computational model. Consider inviscid, compressible flow in a one-dimensional nozzle modeled using a modification of the Euler equations given by

$$\mathbf{w}_t + \mathbf{f}_x(\mathbf{w}) = \mathbf{b}(\mathbf{x}), \tag{2.1}$$

where

$$\mathbf{w} = \begin{bmatrix} \rho \\ \rho u \\ \rho E \end{bmatrix}, \quad \mathbf{f}(\mathbf{w}) = \begin{bmatrix} \rho u \\ (p + \rho u^2) \\ u(p + \rho E) \end{bmatrix}, \quad \mathbf{b}(x) = \begin{bmatrix} 0 \\ pS_x/S \\ 0 \end{bmatrix}, \tag{2.2}$$

in which the y-component of momentum is replaced by a momentum source term, and where the dependent variables have been area weighted, i.e., $S\rho^* = \rho$ and $Sp^* = p$ with asterisked quantities denoting physical values. The system is closed by giving the equation of state for an ideal, polytropic gas:

$$p^* = (\gamma - 1)\rho^*[E - \tfrac{1}{2}u^2], \tag{2.3}$$

where γ is the ratio the specific heat at constant pressure to the specific heat at constant volume for the gas. The equations (2.1)–(2.3) express the conservation of mass (ρ), momentum (ρu), and energy (ρE) and serve to model flow through a Laval nozzle. This system is of interest because it admits nontrivial, steady state solutions which can be computed analytically. The H-system is derived from (2.2) by imposing the total specific enthalpy $H = E + p/\rho$ as constant, yielding a system in which the energy equation is not necessary and the closure relationship involving the pressure is instead given by

$$p^* = \frac{\rho^*}{\gamma}\left[1 - \frac{\gamma - 1}{2}u^2\right]. \tag{2.4}$$

Denoting $\Delta x_{j-1/2} = x_j - x_{j-1}$, a conservative, cell vertex–based finite volume discretization of the problem is constructed using the cell-based residuals $R_{j-1/2} \in (x_{j-1}, x_j)$ given by

$$R(\rho)_{j-1/2} = \frac{(\rho u)_j - (\rho u)_{j-1}}{\Delta x_{j-1/2}}, \tag{2.5}$$

$$R(\rho u)_{j-1/2} = \frac{(p + \rho u^2)_j - (p + \rho u^2)_{j-1}}{\Delta x_{j-1/2}} - \frac{S_x}{2}\left(\frac{p_j}{S_j} + \frac{p_{j-1}}{S_{j-1}}\right), \tag{2.6}$$

$$R(\rho e)_{j-1/2} = \frac{(up + \rho ue)_j - (up + \rho ue)_{j-1}}{\Delta x_{j-1/2}}. \tag{2.7}$$

Note that the momentum source term has been incorporated into the definition of the residual for the momentum. The Lax–Wendroff [14] update is constructed as

$$\delta\mathbf{w}(t + \Delta t) = -\Delta t\ \mathbf{f}_x + \frac{\Delta t^2}{2}\left(\frac{\partial}{\partial x}A\mathbf{f}_x\right). \tag{2.8}$$

Writing the two terms on the right-hand side of (2.8) as $\delta\mathbf{w} = \delta_1\mathbf{w} + \delta_2\mathbf{w}$ and substituting the discrete residual for each component of $\mathbf{f}_x$ yields

$$\delta_1\mathbf{w}_j = -\Delta t\frac{R_{j+1/2}\Delta x_{j+1/2} + R_{j-1/2}\Delta x_{j-1/2}}{\Delta x_{j+1/2} + \Delta x_{j-1/2}} \tag{2.9}$$

and

$$\delta_2\mathbf{w}_j = \frac{1}{2}\Delta t^2\left(\frac{A_{j+1/2}R_{j+1/2} - A_{j-1/2}R_{j-1/2}}{x_{j+1/2} - x_{j-1/2}} + \frac{1}{2}B_j(R_{j+1/2} + R_{j-1/2})\right), \tag{2.10}$$

where $A = \partial \mathbf{f}/\partial \mathbf{w}$ and $B = \partial \mathbf{b}/\partial \mathbf{w}$ are Jacobian matrices. Numerically, A and $\mathbf{f}$ are evaluated at the cell centers, that is, at $j \pm 1/2$, while B is evaluated at the nodal values j. This time iterative algorithm for solving (2.1) converges to a steady state solution when the residual $\mathbf{R}_j$ goes to zero in each cell thereby assuring that $\delta \mathbf{w}_j = \mathbf{0}$ uniquely at each node. This constitutes a one-dimensional implementation of the Ni-type or cell vertex–based finite volume method.

The convergence rates for the Laval nozzle problem are examined for geometries in which the nozzle has cross-sectional height

$$y = 1 - [\vartheta(1 + \cos \pi x)] \qquad x \in (-1, 1), \tag{2.11}$$

depending on ϑ which is used to investigate different combinations of nozzle geometry and inlet conditions. The initial conditions are free stream throughout the nozzle. The inlet Mach numbers are chosen so that the flow remains subsonic throughout the nozzle during the transient, as no artificial damping is introduced to stabilize the LW update (thereby altering the properties of the numerical scheme). Nonreflective boundary conditions are implemented based on a predictor-corrector scheme using Riemann invariants [23] to mitigate the generation of errors at the boundaries. The constant $\gamma = 1.4$ (for air at standard temperature and pressure) is used.

3. Convective and damping properties. Assuming that the system in (2.1)–(2.2) along with (2.3) or (2.4) for the full or H-system, respectively, can be linearized, the equations can be written as a decoupled system of one-dimensional convection equations of the form $\mathbf{v}_t + \Lambda \mathbf{v}_x = \mathbf{c}$ with waves propagating at speeds given by the eigenvalues of the system. For the H-system there are two waves to consider, corresponding to the eigenvalues

$$\xi_s = u - a_s \qquad \text{and} \qquad \xi_f = u + a_f, \tag{3.1}$$

where a_s and a_f are given by

$$a_s = \frac{\gamma - 1}{2\gamma} u + \sqrt{\frac{a^2}{\gamma} + \left(\frac{1-\gamma}{2\gamma} u\right)^2}, \quad a_f = -\frac{\gamma - 1}{2\gamma} u + \sqrt{\frac{a^2}{\gamma} + \left(\frac{1-\gamma}{2\gamma} u\right)^2} \tag{3.2}$$

and where a is the local sound speed. For the full system there are three waves to consider,

$$\xi_{s_1} = u - a, \qquad \xi_{s_2} = u, \qquad \text{and} \qquad \xi_f = u + a. \tag{3.3}$$

For subsonic flows with $u > 0$ (taken throughout in the positive x direction along the nozzle), the fast wave is given by ξ_f for the H-system and the slow wave is given by ξ_s in (3.1)–(3.2). For the full system in (3.3) the fastest wave is always ξ_f and there are two slow waves with the slowest wave depending upon the Mach number, $M = u/a$. If $0.5 < M$, then ξ_{s_2}, while if $0.5 > M$, then ξ_{s_1}.

In computing the time step by which the numerical computation is advanced using the explicit scheme in (2.8), the restriction is to stay within the domain of dependence of the fastest wave. This requires that the CFL number $\nu = \xi \Delta t/h < 1$ be associated with the fast wave, ξ_f.

However, associated with the other waves ξ_s in the H-system and ξ_{s_1} and ξ_{s_2} in the full system are also the wave numbers ν_s, ν_{s_1}, and ν_{s_2}, respectively. Because local time stepping is used to accelerate convergence to steady state, the convective speed

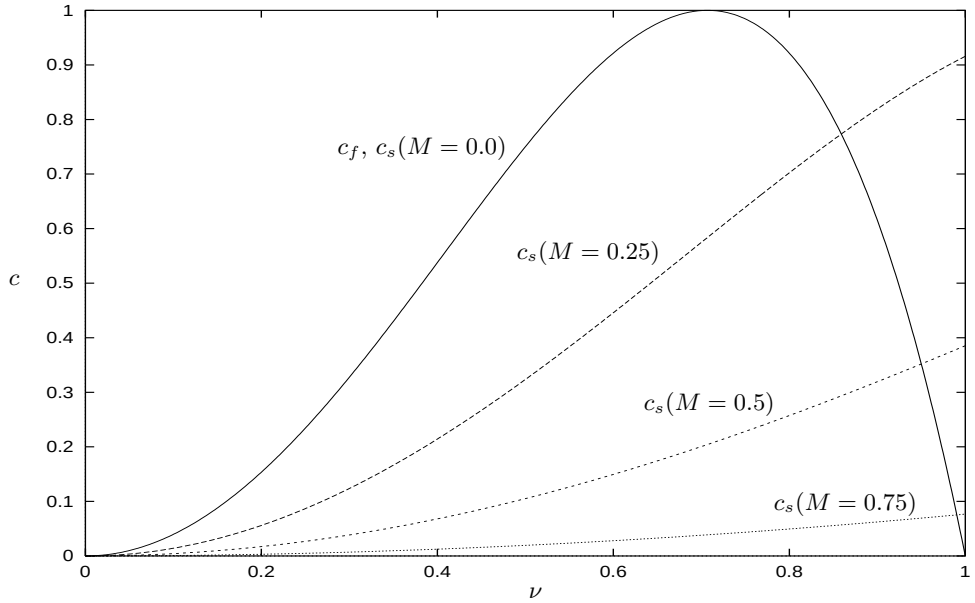

FIG. 3.1. *Damping coefficient for LW as a function of Mach number for modes associated with the fast wave ν_f and slow wave ν_s for the isenthalpic system. If $M = 0$, the damping is exactly the same for both waves. As the Mach number increases the critical value of the CFL number at which the slow wave is damped better than the fast wave increases until at $M = 1.0$, at which point the slow wave is not damped at all.*

of the slow waves varies throughout the domain with the corresponding slow wave CFL number ν_s given by the elementary scaling

$$\nu_s = \nu_f |\xi_s/\xi_f|. \tag{3.4}$$

This affects the amplification and dispersive properties of the computational method. In particular, the effectiveness in damping fast waves when applying the Lax–Wendroff update is different than the effectiveness in damping the slower waves.

Recall that the amplification factor for the Lax–Wendroff update is given by

$$\lambda = \left[1 - c(\nu)\sin^4\left(\frac{\eta h}{2}\right)\right]^{\frac{1}{2}}, \tag{3.5}$$

where h is the mesh spacing, η is the wave number, and c is the wave speed–dependent damping coefficient given by

$$c(\nu) = 4\nu^2(1 - \nu^2). \tag{3.6}$$

Since the wave speed–dependent damping $c(\nu)$ is modulated by the term $\sin^4(\eta h/2)$, at low frequencies, i.e., when $\eta h \to 0$, damping vanishes, while at high frequencies, i.e., when $\eta h \to \pi$, damping is maximized.

Having chosen the CFL number ν_f based on the fast wave, the damping for this wave is given by $c_f = c(\nu_f)$ in (3.6). The damping for the other waves is obtained by scaling the CFL number to the wave speed of the fast wave in (3.4) and the

corresponding value of the damping is computed using $c_s = c(\nu_s)$, as shown in Figure 3.1. Since ξ_s depends only on the local Mach number, the damping of the slow wave is less than the damping of the fast wave, except when the CFL number is greater than some critical value depending on Mach number. For example, if the Mach number $M = 0.5$, then if $\nu > 0.93$ the damping of the slow wave is greater than the damping of the fast wave.

Understanding convergence in many of these cases will be seen to be determined by how well the iterations deal with the slow wave. Despite the crossover of the curves for damping and the need to linearize the original system in order to analyze it, the convergence to steady state can be seen to depend on the effects of nonlinearity on the slow wave; i.e., the convergence process causes the slow wave to become trapped on the domain.

3.1. Eliminating unsteady waves. As an immediate consequence of (3.1)–(3.6), local time stepping introduces a dependence of the slow wave on the local Mach number requiring a knowledge of its variation during the transient in order to estimate the damping and convection of the slow wave. The fast wave in contrast is not dependent on anything but the choice of ν. At steady state, for subsonic flow throughout a converging-diverging Laval nozzle the local Mach number varies from about free stream at the inlet and outlet to a maximum in the interior of the nozzle. Furthermore, this dependence is different for each system and varies less predictably during the initial transient. To handle this, a further linearization assumption is introduced to allow damping and convection to be assessed at a frozen value of the Mach number.

Analysis for the isenthalpic system. Since

$$\left|\frac{\xi_s}{\xi_f}\right| = \frac{-(1+\gamma)M + \sqrt{4\gamma + [(1-\gamma)M]^2}}{(1+\gamma)M + \sqrt{4\gamma + [(1-\gamma)M]^2}}, \tag{3.7}$$

it follows that $|\xi_s/\xi_f|_h$ is a monotonically decreasing function of Mach number; i.e., as the Mach number increases, $|\xi_s/\xi_f|$ decreases, $|\nu_s|$ consequently decreases. Despite this dependence of ν_s on the Mach number, it suffices to consider ν_s taken at the inlet in order to predict the amplification factor λ. There are two situations to consider:

1. Writing ν_{s1} as the value of ν_s at the inlet (or outlet) of the nozzle and ν_{s2} as the value of ν_s at any other point in the domain, if ν_{s1} is much less than one at the inlet or outlet to the subsonic nozzle, then $\nu_{s2} < \nu_{s1}$; hence ν_{s2} is much less than one throughout the nozzle, so that

$$\frac{\lambda_1}{\lambda_2} = \left[\frac{1 - 4\nu_{s1}^2(1-\nu_{s1}^2)}{1 - 4\nu_{s2}^2(1-\nu_{s2}^2)}\right]^{1/2} \approx \frac{1 - 2\nu_{s1}^2}{1 - 2\nu_{s2}^2} \approx 1. \tag{3.8}$$

Thus damping of the slow wave is equally ineffective throughout the nozzle if it is ineffective near the entrance or exit from the nozzle.

2. Even when the range of Mach numbers is large and it is not appropriate to consider ν_{s1} near the boundaries to be very small, the Mach numbers at the inlet and outlet are significant since all transient waves escaping from either end of the nozzle are accelerated as the Mach number approaches the free stream values, and consequently the slow waves are convected and damped at a rate proportional to the inlet and outlet Mach numbers. Since convection or damping at this lower Mach number is greater, this represents an upper bound for the damping rate for the slow wave. If damping is effective, then this controls the rate at which transient waves

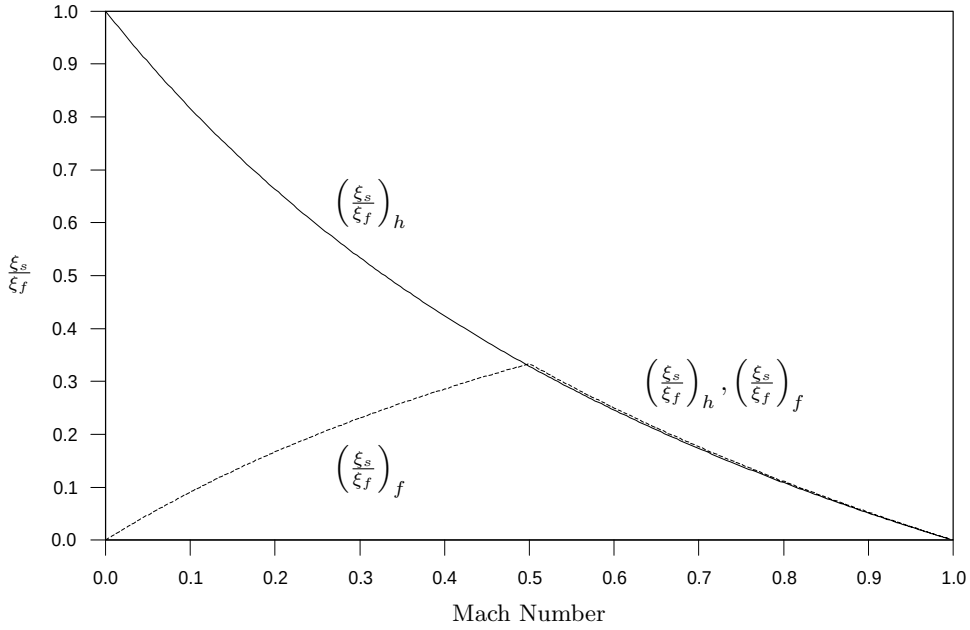

FIG. 3.2. *Comparison of the eigenvalues of the full and H-systems, showing the slowest/fastest eigenvalue.*

are damped. In fact, even during the initial few iterations of the transient, the Mach number at either end tends to dip below the free stream value, enhancing damping of the slow wave in contrast to the interior.

Analysis for the full system. Since

$$\left|\frac{\xi_s}{\xi_f}\right| = \begin{cases} \dfrac{M}{1+M} & \text{if } M \le \dfrac{1}{2}, \\ \dfrac{1-M}{1+M} & \text{if } M > \dfrac{1}{2}, \end{cases} \tag{3.9}$$

the ratio of the eigenvalues has a maximum at $M = 1/2$ and varies in such a way that it is more difficult to easily predict or discern the effects of the slow wave on damping. If $1/2 < M < 1$ throughout the nozzle, the damping decreases monotonically to the sonic point, and the statements made concerning the H-system are equally valid for the full system since for $\gamma = 1.4$,

$$|\xi_s/\xi_f|_h = \frac{\sqrt{\frac{35}{36} + \frac{1}{36}M^2} - M}{\sqrt{\frac{35}{36} + \frac{1}{36}M^2} + M} \approx \frac{1-M}{1+M} = |\xi_s/\xi_f|_f, \tag{3.10}$$

showing that $(\xi_s/\xi_f)_h \approx (\xi_s/\xi_f)_f$ if $M > 1/2$ as shown in Figure 3.2.

If $0 < M \le 1/2$ the variation is again monotonic; however, it is now seen to be increasing and quite the opposite holds with the damping being more effective in the interior of the domain of a converging-diverging nozzle. If the Mach number varies from less than $1/2$ to more than $1/2$, then more detailed knowledge of the Mach number is necessary to correctly predict the scaling of the convergence due to damping of the slow wave. But in any case, a clear implication of Figure 3.2 is that

the full system is less effective at damping unsteady waves at low Mach numbers than the H-system.

Since convergence estimates depend on the rate of elimination of transient waves, suitable working estimates for the Laval nozzle problem can be obtained for those limiting cases where a particular wave provides a bottleneck to the convergence process and yet the coupling between distinct waves is not so large as to influence the rate of convergence (i.e., the linearized eigenvalue model holds in the first place). Because the rates at which waves are convected and damped are competitive processes, their combined effects are often difficult to distinguish, requiring the solution of a nonlinear, related rate problem. Thus limiting cases are investigated.

1. *Damping dominated convergence.* Damping tends to dominate convection as a removal mechanism whenever the amplification factor $\lambda(\nu) \ll 1$; i.e., $c(\nu)$ is uniformly large for all wave numbers η. This is because the amplification factor goes as $\lambda^n(\nu)$ while convection is proportional to $n\nu$. Since $c(\nu)$ is modified by the wave number term $\sin^4(\eta h/2)$, damping controls the rate at which convergence to steady state occurs only on very coarse meshes. However, when the number of grid points is small, convection becomes a competitive mechanism for removing unsteady waves, since the boundaries are near the interior of the domain. This is especially true for the fast wave ξ_f which is convected a distance of exactly one cell at each iteration using local time stepping. In contrast, the convection of the slow wave ξ_s (which slows down as the Mach number increases in the interior, near the converging section of the nozzle) does not compete effectively with damping as a removal mechanism. Thus the damping of the slow wave is controlling.

2. *Convection limited convergence.* In this situation damping is saturated because the computational stencil has damped those (high frequency) modes which can be damped; however, there are still (low frequency) modes available which cannot be damped effectively. Hence the convergence rate is limited by the rate at which convection removes undamped, unsteady waves. Since the convection rate of the slow wave decreases as the Mach number increases, the convection of the slow wave is controlling.

3.2. Convecting unsteady waves. In the absence of any damping a linear wave associated with the eigenvalue ξ travels a distance of $n\xi\Delta t$ in n iterations on a uniform mesh h. This can be written as $n\nu L/N$, where L is the total length of the domain and N is the number of mesh intervals in L. Any two waves travel the same convective distance on the same domain with length L if

$$n_1 \frac{\nu_1}{N_1} = n_2 \frac{\nu_2}{N_2}, \tag{3.11}$$

so that ν/N defines a convective scale factor for the number of iterations n. Assuming a linear convection problem, solved ideally using a numerical update which introduces no dissipation, the wave will be at exactly the same position on the domain after n iterations for any combination of values of mesh N and CFL number ν which yield the same values for $n\nu/N$. Exactly the same convective path is taken by a transient wave. Similarly, on given domain L using LW to solve the Laval nozzle problem, substantial agreement of the convergence histories obtained at different values of ν and N but plotted using a convective scale support the contention that convection is occurring at the same rate in both runs. If the damping predicted by the values of ν are substantially different in these cases, then convection is apparently a controlling

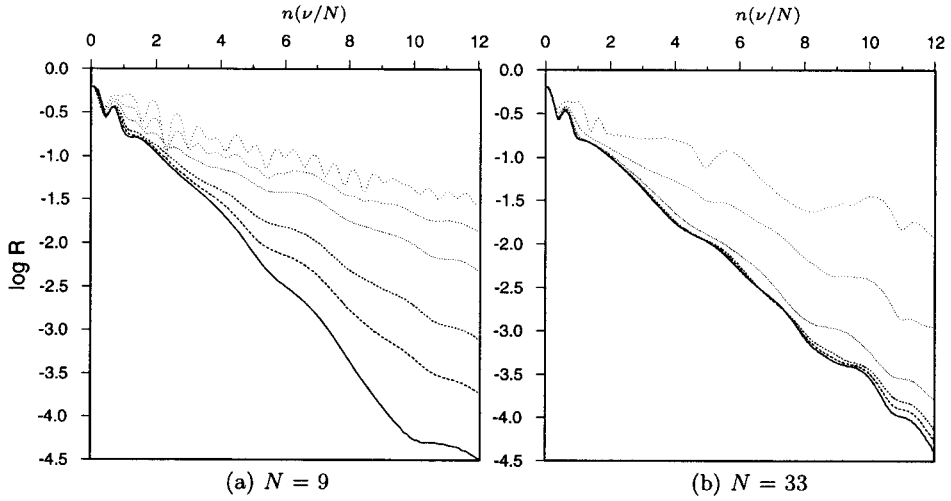

FIG. 3.3. *Plotting convergence for the H-system using increasing values of ν, a convective scale for subsonic flow through a Laval nozzle. The convergence rates on a mesh with* (a) $N = 9$ *and* (b) $N = 33$ *show that* (a) *increasing ν serves to increase the damping, while* (b) *increasing ν serves to increase the damping only up to a given point beyond which damping no longer has any appreciable effect. The value of ν increases with line density, starting with $\nu = 0.02$ displayed as a dotted line, through* 0.1, 0.243, 0.5, 0.71, *ending with $\nu = 0.97$ displayed as a solid line.*

mechanism for removing unsteady waves. For LW this can be expected to occur whenever the mesh is sufficiently refined.

To illustrate this point, consider the convergence of the H-system. In Figure 3.3 the convergence histories for the norm of the residual R have been plotted using a convective scale, $n\nu/N$. For example, at $n = 450$ iterations using local time stepping with $\nu = 0.02$ and $N = 9$, $n\nu/N = 1$. A wave convected along by the LW update using $\nu = 0.71$ instead would have traveled the same distance on the same mesh when $n = N/\nu = 9/0.71 = 12.6 \approx 13$. Consequently, assuming linear, decoupled convection, the solutions should look identical at this point during the transient if convection becomes a dominant removal mechanism.

In Figure 3.3(a) on a very coarse mesh with $N = 9$, LW appears effective at damping all transient modes with the convergence history changing dramatically as ν is increased from 0.02 to 0.97. In contrast, in Figure 3.3(b) the mesh is increased to $N = 33$ on the same domain. As ν is increased the damping is seen to increase as before, however, it now appears to saturate as ν rises above about 0.243 such that when $\nu \geq 0.5$, the graph of R as a function of n traces almost the same lines for $\nu = 0.5$, 0.71, and 0.97 using a convective scale. Increasing ν increases the damping of high frequency modes. The remarkable *self-similarity* of the curves for $\nu = 0.5$, 0.71, and 0.97 supports the interpretation that increasing the damping term is less effective because of the term $\sin^4(\eta h/2)$ in the amplification factor. Damping appears to be ineffective above the threshold value of $\nu \approx 0.5$, and the error is diminishing at a rate consistent with linear convection model in (3.11). While damping is important (otherwise the slope of the trace of the residual curve would decrease), the remarkable self-similarity of the trace of the convergence history curve for the residual for larger values of ν shows clearly the imprint of convection with almost exactly the same path taken to the converged solution in Figure 3.3(b) for ν large.

4. Numerical experiments. Consider the convergence to steady state in which each of the cell residuals approaches zero. If unsteady waves are reduced by a factor λ in amplitude on each iteration, the convergence after n iterations is

$$\mathsf{R} = K\lambda^n, \tag{4.1}$$

where K is a constant to be determined and R is taken to be the norm of the residual, $\mathsf{R} \equiv ||R||$. Since the convergence to steady state is taking place on a finite domain, K will include the effects of removal at the boundary by convection as well as the effects of the generation of numerical errors which are not modeled by the analytic expression for the amplification factor, λ. From the observed convergence rate the observed amplification factor is computed using

$$\Delta \log \mathsf{R} = \Delta \log K + n \log(\lambda). \tag{4.2}$$

The value of $\Delta \log K$ is obtained from numerical studies by taking ν_f and consequently ν_s sufficiently small, thereby letting $\log(\lambda) \to 0$. Using a best least squares line fit to the data $\{(j, \mathsf{R}_j)\}$ along with (4.2) yields on taking $\lim \nu_f \to 0$,

$$\Delta \log K = \Delta \log \mathsf{R}, \tag{4.3}$$

providing an effective and practical means for estimating K numerically and for removing the effects of convection from the analysis.

4.1. The slow wave. In investigating the convergence of the LW update and its relationship to the eigenvalues of the modeled system a dramatic visualization is afforded by plotting the residual (2.5) at each point along the nozzle, x_j, $j = 1, \ldots, N$, at each iteration n as shown in Figure 4.1. In this case the convergence of the H-system is examined, starting with the initial transient at iteration $n = 0$. In this perspective graph, the initial distribution of $R_j(\rho u)$ is shown in the far field at the back of the rectangular region in the (x, n)-plane, with the number of iterations n increasing in the direction of the near field. The inlet boundary to the nozzle is on the right-hand side, and the flow is in the direction of the positive x-axis with x increasing as shown.

Initially, there is a large long-wavelength oscillation in the residual tracing the flux across the domain. Since the initial condition is taken to be free stream throughout the nozzle the initial amplitude of the disturbance is expected to be large. As the solution evolves with n increasing, only the wave which originates at the outlet boundary on the left is visible. This wave is observed to slow down near the center of the nozzle where the curvature of the trace of the wavefront at the crest of the wave, instead of tracing a straight line path across the $x \times n$ domain, curves to become nearly a standing wave in the middle of the nozzle. Since the local time step is based on the fast wave, the trace of information moving along with ξ_f and hence indirectly with the residual would show the wave front moving one mesh point each iteration corresponding to ν_f which in this case is near one. (The trace of the slow wave depends on the factor ξ_s/ξ_f, which depends on the local value of the Mach number.) The point is that as M increases, the slow wave speed ν_s decreases, corroborating the point that the slowing down of the slow wave controls the convergence rate.

From Figure 3.3(b) it was observed that at a value of $\nu = 0.97$, $N = 33$, the damping is saturated for the H-system. The elimination of the residual is clearly visualized (Figure 4.1). Damping and convection play a significant role in reducing the initial transient; however, after the initial transient has passed, the wavefronts

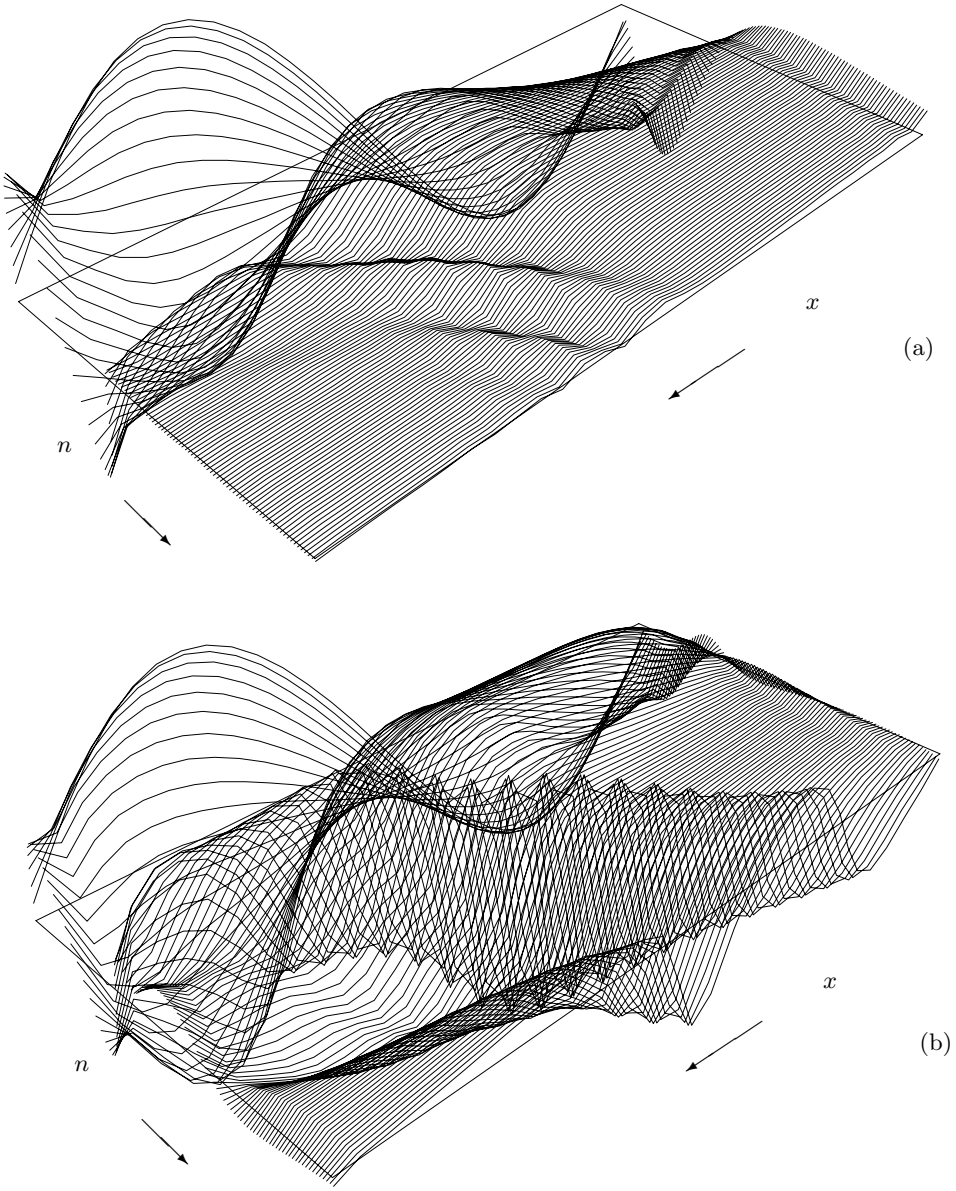

FIG. 4.1. *The residual along the nozzle,* x*, plotted against the number of iterations,* n*, obtained using* (a) *nonreflective boundary conditions and* (b) *a well-posed but reflective boundary condition, pressure. The number of iterations shown is* 100*, and* $\nu = 0.97$ *with* $N = 33$*.*

which are visible in Figure 4.1 are entirely those belonging to the slow moving wave. Incidentally, since the slow wave corresponds to the $u - a_s$ eigenvalue of the system, this wave is expected to move in the negative x direction, as observed. The figure shows clearly that the movement of the slow wave has stalled while at the same time it is not being damped significantly.

In the subsonic region if the Mach number is increasing, the velocity of the slow wave is decreasing. In this example, since the Mach number near convergence is 0.8

TABLE 4.1

Convergence of the Laval nozzle problem for the H-system. The value of λ_{obs} is the observed amplification factor and $\lambda_p(\nu_s)$ is the amplification predicted based on using $\nu_s = (\xi_s/\xi_f)\nu_f$ in (3.5) for 9, 17, and 33 mesh points.

		$N = 9$		$N = 17$		$N = 33$	
ν_f	ν_s	λ_{obs}	$\lambda_p(\nu_s)$	λ_{obs}	$\lambda_p(\nu_s)$	λ_{obs}	$\lambda_p(\nu_s)$
0.02	0.00848	0.9999	0.9998	0.9999	0.9999	0.9999	1.0000
0.1	0.0424	0.9982	0.9991	0.9989	0.9995	0.9989	0.9998
0.243	0.103	0.9931	0.9947	0.9954	0.9973	0.9962	0.9987
0.5	0.212	0.9772	0.9783	0.9865	0.9892	0.9911	0.9946
0.71	0.301	0.9604	0.9579	0.9789	0.9792	0.9870	0.9896
0.97	0.411	0.9246	0.9271	0.9694	0.9643	0.9813	0.9822

at the center of the nozzle, the slow wave near the center is moving at only about 1/9 the speed of the fast wave compared to about 1/4 the speed of the fast wave near the boundaries where the Mach number is about 0.4. The damping of the slow wave which also depends on the Mach number is also less effective near convergence, being about 1/5 as effective as near the boundaries. Consequently the slow wave is trapped in the interior of the domain.

If this numerical experiment is repeated with a slightly higher initial free stream Mach number, the flow will go sonic in the throat of the nozzle. As the sonic line forms in the throat of the nozzle, the residuals at this point become trapped since

$$\lim_{M\to 1} \nu_s = \lim_{M\to 1} \left(\frac{\xi_s}{\xi_f}\right) \nu_f = 0. \tag{4.4}$$

Thus the damping and convection of the residual vanish as $M = 1$ and convergence (i.e, $||R|| \to 0$) cannot be achieved. Adding additional dissipation (artificial viscosity) allows for the removal of this stationary wave. This observed phenomenon is a manifestation of transient, nonlinear wave propagation [17].

To demonstrate in part that this nonlinear wave behavior of the residual is independent of the boundary conditions (and incidentally to illustrate the significance of using nonreflective boundary conditions) the reflected error wave is examined using a boundary condition based on Riemann invariants at the outlet in contrast to using pressure as the outlet boundary condition. Imposing the pressure, while well posed, is known to reflect waves back at the outlet boundary [20]. At the inlet nonreflective boundary conditions are applied uniformly. Figure 4.1(a) illustrates the convergence of Lax–Wendroff update with $\nu = 0.97$ using nonreflective boundary conditions at the outlet boundary, while in Figure 4.1(b) pressure is imposed at the outlet boundary. In both of these figures the absolute magnitude of the initial transient is the same, however the upstream traveling wave depicted moving from left to right is substantially greater in magnitude when pressure is imposed. The shape, direction, and slowing down of this wave are very similar to the discussion of the case in Figure 4.1(a).

4.2. Damping limited convergence and the role of the slow wave. Numerical results obtained using the H-system confirm the role of the slow wave ξ_s corresponding to the CFL number ν_s in controlling the rate of convergence to steady state. The effects of damping on the slow wave are assessed by experimentally eliminating the effects of convection. This is exemplified in Table 4.1, tabulating the results

obtained with $\vartheta = 0.1$ using a free stream Mach number of 0.4. In these the CFL number ν_f associated with the fast wave ξ_f is varied for several uniformly spaced meshes. This is the CFL number which is used to advance the computation on each time step in each cell. The number ν_s for the slow wave corresponding to each choice of ν_f is tabulated alongside ν_f. The table shows the observed amplification factor obtained from numerical studies in which ν_f is varied, compared to the predicted amplification factor λ_p obtained using ν_s on uniform meshes of $N = 9$, 17, and 33 points. The agreement between $\lambda_p(\nu_s)$ and the observed value of λ is quite good.

In contrast, consider computing $\lambda_p(\nu_f)$, that is, predicting the amplification factor using the fast wave CFL number. From (3.5) the amplification factor for the fast wave has a minimum at $\nu_f = 0.71$, which is very nearly zero, while the observed amplification factor is greater than 0.96 in all cases. In addition, the damping at wave speeds corresponding to $\nu_f = 0.243$ and $\nu_f = 0.97$ should be about equal in magnitude, as can be seen from Figure 3.1. None of this fast wave damping is observed. In comparing the numerical results to prediction, the damping predicted by using the slow wave, which is a slowly increasing function of ν_s, is consistent with the observed decay of the transient solution. Indeed, since the convergence rate is unaffected by the choice of CFL number for the fast wave, the fast wave imposes no limits as a result of damping or convection on the convergence process. The convergence rate is limited by the rate at which unsteady, slow waves are being removed from the domain.

If the free stream Mach number is taken to be sufficiently small, then the velocities through the Laval nozzle remain very close to the original inlet velocity for a given value of ϑ. Under these circumstances, the competition between damping of the fast and slow waves becomes less pronounced, consistent with the expected behavior of $(\xi_s/\xi_f)_h$ shown in Figure 3.2. Repeating the numerical studies summarized in Table 4.1, using instead lower free stream Mach numbers, the difference in convergence rates for different values ν is found to decrease. There is very little difference between the fast wave and the slow wave for the H-system, and the constraint imposed by the CFL number in choosing ν_f is equally effective at expelling either wave by convection and damping since $\nu_f \approx \nu_s$. Similarly, if the value of ϑ is taken to be sufficiently small, the Mach number throughout the nozzle remains close to the free stream value at the inlet. Using a free stream value of $M = 0.4$ along with $\vartheta = 0.1$ represents an extreme since the flow just barely stays subsonic in the throat under these conditions. As ϑ is increased much above this, and the free stream Mach number is decreased to maintain subsonic flows, it becomes more difficult to accept freezing the Mach number dependency of the slow wave at a single value.

As noted, transient waves with long wavelengths are not damped effectively by LW. If damping is ineffective, the dependence of the average amplification factor $\bar{\lambda}$ on the wave number η as the mesh is refined can be estimated assuming an equi-distribution of modes,

$$\bar{\lambda} = \frac{1}{N}\sum_{n=1}^{N} \lambda(\xi_n) = \frac{1}{N}\sum_{n=1}^{N} \left[1 - c\sin^4\left(\frac{\pi}{n}\right)\right]^{1/2} \tag{4.5}$$

$$\approx 1 - \frac{c}{2N}\sum_{n=1}^{N} \sin^4\left(\frac{\pi}{n}\right). \tag{4.6}$$

Consequently, for N sufficiently large,

$$\bar{\lambda}(N) \approx 1 - \frac{c}{N}. \tag{4.7}$$

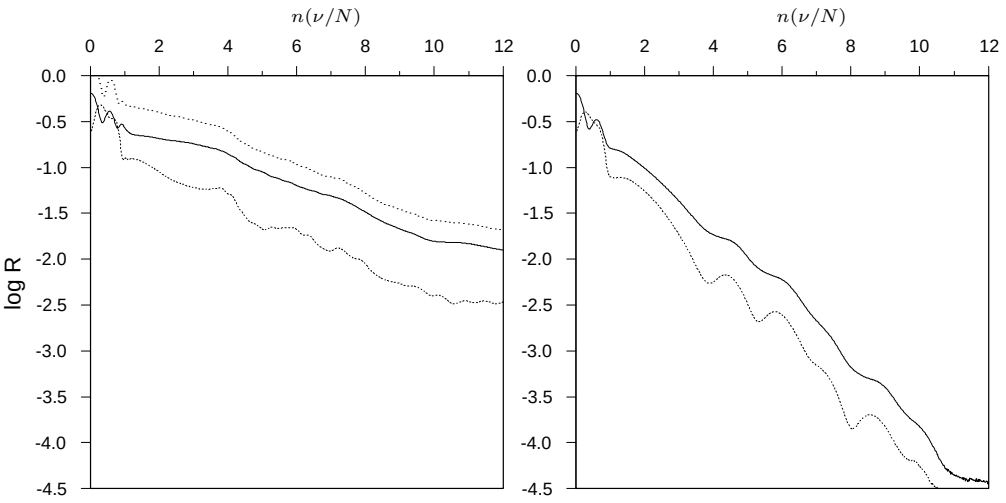

(a) Full system (b) Isenthalpic system

FIG. 4.2. *Comparison of the convergence rates at* $N = 65$ *with* $\nu = 0.97$ *showing the residual of* $\mathsf{R}(\rho)$, $\mathsf{R}(\rho u)$, *and* $\mathsf{R}(\rho e)$ *shown in solid, dashed, and dotted lines (for the full system only) and* $M_\infty = 0.4$.

The $1/N$ decrease in the damping term as the mesh is refined is incorporated in the term $\sin^4(\eta h/2)$ used to construct λ_p. For example, a value of 0.25 fit the data on a mesh of 9 points, consequently 0.125 and 0.0625 are used to fit the results obtained on a mesh 17 and 33 points. As the mesh is refined, the solution mechanism becomes increasingly dependent on convection for removing transient waves from the domain. Examining Table 4.1, the success in accurately predicting the damping decreases as N increases. Since fewer modes are being effectively damped, convergence to steady state is increasingly dominated by the rate at which these modes can be convected from the domain, making the asymptotic estimate of K more important.

4.3. The isenthalpic and full systems. The increase in the convergence rate which is observed when solving the H-system compared to the full Euler system of equations using LW is illustrated in Figure 4.2. Experiments with using the H-system and the full system for solving transonic flow problems involving one- and two-dimensional internal flows using local time stepping lends support to the contention that the H-system decreases the cost of achieving converged solutions. Steady state solutions are obtained several times faster, ranging anywhere from a factor just above 1 to an order of magnitude better. The results for the H-system agree well with the full system at convergence.

In the case of the full Euler equations, there are three eigenvalues instead of the two eigenvalues for the H-system. Again, because of local time stepping, the damping and convection of the three waves depend on the CFL number which is chosen to accommodate the fastest wave and any bottlenecks to convergence will tend to occur because of the slowest wave. In contrast though to the H-system, the Mach number dependence does not vanish as $M \to 0$. Both damping and convection of the slow wave are affected more than for the H-system, especially for low Mach number flows. Thus in assessing these comparatively, the focus was on fine mesh models which favor convection-limited convergence.

If the values of $(\xi_s/\xi_f)_h$ and $(\xi_s/\xi_f)_f$ were the only factors contributing to a determination of the convergence rates of the isenthalpic and full systems, then using Figure 3.2 this difference can be expected to increase as the Mach number is decreased below 0.5. Similarly this difference can be expected to decrease as the Mach number increases and the two methods can be expected to produce the same convergence rates above a Mach number of 0.5. For problems in which convection of unsteady waves from the domain is the dominant means by which convergence to steady state is achieved, the convergence rate of the H-system relative to the full system should scale as

$$d = \frac{\left(\frac{\xi_s}{\xi_f}\right)_h}{\left(\frac{\xi_s}{\xi_f}\right)_f}. \tag{4.8}$$

This is indeed the situation on sufficiently fine meshes on which convection limited flows would be expected to occur. Using a free stream Mach number of 0.1, the H-system converges about 10 times faster than the full Euler equations. This is consistent with a value of $d \approx 0.82/0.09 = 9$. For the problem with an incoming Mach number of 0.4, the factor for the relative convergence rates of the two systems should be about $0.42/0.29 = 1.5$. In fact the observed rate of convergence of the H- to the full system is about 3; i.e., the H-system converges about 3 times faster than the full system.

Using a value of $\vartheta \leq 0.1$ in (2.11), the flow remains subsonic in the nozzle at larger Mach numbers. Choosing $\vartheta = 0.05$, and repeating the comparison between the H- and full systems, using free stream Mach numbers below 0.5, similar results are obtained in the relative scaling of the two systems. That is, at a Mach number of 0.1, the H-system converges about 10 times faster than the full Euler, which is consistent with the expected value. Increasing the free stream Mach number to 0.4 reduces the observed convergence rates scaling by a factor of about 3. Using Mach numbers of 0.5, this factor stays at about 2.

Further numerical experiments confirm that although the trend is correct, the numbers do not scale perfectly, especially as the free stream Mach number increases above 0.5. On the other hand, at low Mach numbers the predictions are in substantial agreement with observations. This is not surprising, since at the higher Mach numbers, the assumptions implicit in the linearization and decoupling of the systems become increasingly invalid and it becomes increasingly hazardous to predict relative rates of convergence based on assuming a frozen Mach number. In particular, the damping in the Lax–Wendroff update is important and is occurring in either system in an independent fashion. Since the convergence rates of the H-system are higher than predicted by the convection model, damping, which is more effective in the H-system for the slow wave, may contribute to the observed discrepancies. Nevertheless, it is interesting just how successful such a simple approach can be in scoping the comparative behavior of these systems.

5. Conclusion. By examining and analyzing the eigenvalues of the linearized isenthalpic and full systems of equations, a revealing picture of the role of damping and convection as competitive mechanisms for removing unsteady waves can be built up. Although this approach would clearly break down in the case when the problem becomes strongly nonlinear, its application to model problems which are only weakly nonlinear does appear to have merit and can provide insight into the solution mechanism.

In the case of the Euler equations involving flow in a simple geometry, the role of the slow waves in limiting both of these mechanisms is seen to be critical in determining the performance of LW when local time stepping is used. An interesting observation is that the purpose in going to local time stepping is to improve the rate of convergence of LW. Unfortunately, this does nothing to affect the reduction in the effectiveness of the damping and convection of the slow wave as the Mach number increases. Ideally for optimal convergence each wave needs to be convected independently at its own CFL limit, which is a strong argument for upwind methods.

Significantly, the speed-up of the isenthalpic system is found to be Mach number dependent, showing the greatest improvement over the full system at very low Mach numbers and the least improvement at high Mach numbers. Since the isenthalpic system is introduced to solve problems involving transonic flows, the inescapable conclusion is that the improvement is least significant when it is most desired. Nevertheless, from the results and analysis of the isenthalpic system at low Mach numbers the lesson is clear that it is important, when possible, to tightly band the eigenvalues of the system.

Characteristically, on realistic computational grids damping is an inefficient mechanism in LW, increasing the significance of well-designed and implemented nonreflective boundary conditions, and the importance of schemes like multigrid in damping transients. While multiple grid methods which were introduced into explicit, pseudo–time stepping, finite volume schemes do not fall neatly into the theory of multigrid, the role of improving the damping of the slow wave by shifting it onto a coarse grid and simultaneously improving the convection rate is important given the inadequacy of this process on the fine grid, especially for the slow wave.

Finally, plotting convergence results on a scale measured in units of $n\nu/N$ effectively demonstrates when damping has slowed substantially and reliance on convection becomes necessary to expel waves which are inconsistent with the steady state. If nothing else, plotting convergence histories this way is surprisingly revealing.

REFERENCES

[1] A. Brandt, *Multi-level adaptive solutions to boundary value problems*, Math. Comp., 31 (1977), pp. 333–390.

[2] B. Engquist and A. Majda, *Absorbing boundary conditions for the numerical simulation of waves*, Math. Comp., 31 (1977), pp. 629–651.

[3] M. Giles, *Eigenmode Analysis of Unsteady One-Dimensional Euler Equations*, Paper NASA-CR-172217, ICASE, Langley Research Center, Hampton, 1983.

[4] M. Giles, *Non-Reflecting Boundary Conditions for the Euler Equations*, Paper CFDL-TR-88-1, Massachusetts Institute of Technology, Cambridge, MA, 1988.

[5] M. G. Hall, *Cell-vertex multigrid schemes for solution of the Euler equations*, in Proceedings of the Conference on Numerical Methods for Fluid Dynamics, University of Reading, K. W. Morton and M. J. Baines, eds., Oxford University Press, Oxford, UK, 1985, pp. 303–345.

[6] G. W. Hedstrom, *Nonreflecting boundary conditions for nonlinear hyperbolic systems*, J. Comput. Phys., 30 (1979), pp. 222–237.

[7] A. Jameson, *Acceleration of Transonic Potential Flow Calculations on Arbitrary Meshes by the Multiple Grid Method*, Paper 79-1458, AIAA, New York, 1979.

[8] A. Jameson, *Transonic aerofoil calculations using the Euler equations*, in IMA Conference on Numerical Methods in Aeronautical Fluid Dynamics, P. L. Roe, ed., Academic Press, London, 1981, pp. 289–308.

[9] A. Jameson, *Transonic Flow Calculations*, MAE report 1651, Princeton University, Princeton, NJ, 1983.

[10] A. Jameson and D. Mavriplis, *Finite volume solution of the two-dimensional Euler equations on a regular triangular mesh*, AIAA J., 24 (1986), pp. 611–618.

[11] A. Jameson, W. Schmidt, and E. Turkel, *Numerical Solutions of the Euler Equations by Finite Volume Methods Using Runge–Kutta Time Stepping*, Paper 81–1259, AIAA, New York, 1981.

[12] G. M. Johnson, *Multiple-Grid Acceleration of Lax–Wendroff Algorithms*, Technical memorandum 82843, NASA, Lewis Research Center, Cleveland, OH, 1982.

[13] G. M. Johnson, *Multiple-grid convergence acceleration of viscous and inviscid flow computations*, Applied Math. Comput., 13 (1983), pp. 375–398.

[14] P. D. Lax and B. Wendroff, *Difference schemes for hyperbolic equations with high order of accuracy*, Comm. Pure and Appl. Math., 17 (1964), pp. 381–398.

[15] K. W. Morton and M. F. Paisley, *A finite volume scheme with shock fitting for the steady Euler equations*, J. Comput. Phys., 80 (1989), pp. 168–203.

[16] R.-H. Ni, *A Multiple Grid Scheme for Solving the Euler Equations*, Paper 81-1025, AIAA, New York, 1981.

[17] P. Prasad, *Nonlinear wave propagation on an arbitrary steady transonic flow*, J. Fluid Mech., 57 (1973), pp. 721–737.

[18] P. L. Roe and B. van Leer, *Non-existence, non-uniqueness and slow convergence in discrete conservation laws*, in Numerical Methods for Fluid Dynamics III, K. W. Morton and M. J. Baines, eds., Oxford University Press, Oxford, 1988, pp. 520–529.

[19] C. Rossow, *Comparison of cell centered and cell vertex finite volume schemes*, in Proceedings of the Seventh GAMM-Conference on Numerical Methods in Fluid Mechanics, M. Deville, ed., Notes Numer. Fluid Mechanics 20, Fried. Vieweg & Sohn, Braunschweig, 1988, pp. 327–334.

[20] D. H. Rudy and J. C. Strikwerda, *A nonreflecting outflow boundary condition for subsonic Navier–Stokes calculations*, J. Comput. Phys., 36 (1980), pp. 53–70.

[21] J. Steinhoff and A. Jameson, *Multiple solutions of the transonic potential flow equation*, AIAA J., 20 (1982), pp. 1521–1525.

[22] L. N. Trefethen, *Group velocity interpretation of the stability theory of Gustafsson, Kreiss, and Sundström*, J. Comput. Phys., 49 (1983), pp. 199–217.

[23] W. J. Usab, Jr. and E. M. Murman, *Embedded mesh solution of the Euler equation using a multiple-grid method*, in Advances in Computational Transonics, W. G. Habashi, ed., Recent Advances in Numerical Methods in Fluids 4, Pineridge Press, Swansea, 1985, pp. 447–472.

[24] J.-P. Veuillot and H. Viviand, *Pseudo-unsteady method for the computation of transonic potential flows*, AIAA J., 17 (1979), pp. 691–693.

[25] J.-P. Veuillot and H. Viviand, *Computation of steady inviscid transonic flows using pseudo-unsteady methods*, in Numerical Methods for the Computation of Inviscid Transonic Flows with Shock Waves, GAMM Workshop 3, A. Rizzi and H. Viviand, eds., Fried. Vieweg & Sohn, Braunschweig, 1981, pp. 45–57.

[26] R. Vichnevetsky, *Wave propagation analysis of difference schemes for hyperbolic equations: A review*, Internat. J. Numer. Methods Fluids, 7 (1987), pp. 409–452.

[27] R. Vichnevetsky and J. B. Bowles, *Fourier Analysis of Numerical Approximations of Hyperbolic Equations*, SIAM Stud. Appl. Math., SIAM, Philadelphia, 1982.

[28] H. Viviand, *Pseudo-unsteady systems for steady inviscid flow calculation*, Paper 1984-69, ONERA, 1984, Séminaire INRIA "Méthodes numériques pour les équations d'Euler pour les fluides parfaits compressibles," Rocquencourt, 7–9 décembre, 1983.